Measurement report: Method for evaluating CO_2 emissions from a cement plant using atmospheric $\delta(O_2/N_2)$ and CO_2 measurements and its implication for future detection of CO_2 capture signals

Shigeyuki Ishidoya[1], Kazuhiro Tsuboi[2], Hiroaki Kondo[1], Kentaro Ishijima[2], Nobuyuki Aoki[1], Hidekazu Matsueda[2], and Kazuyuki Saito[3]

[1]National Institute of Advanced Industrial Science and Technology (AIST), Tsukuba 305-8569, Japan,
[2]Meteorological Research Institute, Tsukuba, Japan, Tsukuba305-0052, Japan,
[3]Japan Meteorological Agency, Tokyo, Japan, Tokyo 105-8431, Japan

Correspondence to: Shigeyuki Ishidoya (s-ishidoya@aist.go.jp)

Abstract. Continuous observations of atmospheric $\delta(O_2/N_2)$ and CO_2 amount fractions have been carried out at Ryori (RYO), Japan since August 2017. In these observations, the O_2:CO_2 exchange ratio (ER, $-\Delta y(O_2)\Delta y(CO_2)^{-1}$) has frequently been lower than expected from short-term variations in emissions from terrestrial biospheric activities and combustion of liquid, gas, and solid fuels. This finding suggests a substantial effect of CO_2 emissions from a cement plant located about 6 km northwest of RYO. To evaluate this effect quantitatively, we simulated CO_2 amount fractions in the area around RYO by using a fine-scale atmospheric transport model that incorporated CO_2 fluxes from terrestrial biospheric activities, fossil fuel combustion, and cement production. The simulated CO_2 amount fractions were converted to O_2 amount fractions by using the respective ER values of 1.1, 1.4, and 0 for the terrestrial biospheric activities, fossil fuel combustion, and cement production. Thus obtained O_2 and CO_2 amount fraction changes were used to derive simulated ER for comparison with the observed ER. To extract the contribution of CO_2 emissions from the cement plant, we used $y(CO_2^*)$ as an indicator variable, where $y(CO_2^*)$ is a conservative variable for terrestrial biospheric activities and fossil fuel combustion obtained by simultaneous analysis of observed $\delta(O_2/N_2)$ and CO_2 amount fractions and simulated ERs. We confirmed that the observed and simulated ER values and also the $y(CO_2^*)$ values and simulated CO_2 amount fractions due only to cement production were generally consistent. These results suggest that combined measurements of $\delta(O_2/N_2)$ and CO_2 amount fractions will be useful for evaluating CO_2 capture from flue gas at carbon capture and storage (CCS) plants, which, similar to a cement plant, change CO_2 amount fractions without changing O_2 values, although CCS plants differ from cement plants in the direction of CO_2 exchange with the atmosphere.

1 Introduction

Simultaneous analysis of atmospheric $\delta(O_2/N_2)$ and CO_2 amount fractions has been used to estimate the global CO_2 budget since the early 1990s (e.g. Keeling and Shertz, 1992). Recently, these analyses have also been applied to separate the contributions of different sources to the local CO_2 budget in an urban area (e.g. Ishidoya et al., 2020; Sugawara et al., 2021; Pickers et al., 2022; Liu et al., 2023). This approach uses $-O_2$:CO_2 exchange ratios (ER, $-\Delta y(O_2)\Delta y(CO_2)^{-1}$) for terrestrial

35 biospheric activities and fossil fuel combustion. For terrestrial biospheric O_2 and CO_2 fluxes, ERs of 1.1 or 1.05 are generally used (Severinghaus, 1995; Resplandy et al., 2019), and for the fluxes due to fossil fuel combustion, ERs of 1.95 for gaseous fuels, 1.44 for oil and other liquid fuels, 1.17 for coal and other solid fuels, and 0 for cement production are typical (Keeling, 1988). Therefore, atmospheric O_2 amount fraction varies in opposite phase with CO_2 amount fraction, owing to terrestrial biospheric activities and fossil fuel combustion. The ERs are typically very stable, and the global average ER for fossil fuels

40 is about 1.4 (e.g. Keeling and Manning, 2014). It is noted that the words "Oxidative Ratio (OR)" has also been widely used in by the same definition as ER. Strictly speaking, there is a distinction in the terminology between ER and OR; the ER indicates the exchange between the atmosphere and organisms or ecosystems while the OR indicates the stoichiometry of specific materials (Faassen et al., 2023). We use the ER throughout the present study conveniently, but the distinction should be kept in mind.

45   In the cement production process, calcium carbonate is burned and calcium oxide and CO_2 are produced as follows:

$$CaCO_3 \rightarrow CaO + CO_2. \hspace{3cm} (1)$$

Because this chemical reaction emits CO_2 to the atmosphere without O_2 consumption, its ER is 0. It should be noted that

50 the cement kilns are usually fired with fossil fuels, so that the overall ER for cement production is not 0. CO_2 emissions from cement production account for about 2 % of global fossil fuel CO_2 emissions (Friedlingstein et al., 2022). However, because it is difficult to separate the cement production signal from CO_2 emissions due to fossil fuel combustion and terrestrial biospheric activities, no study has reported direct evidence of variations in the atmospheric CO_2 amount fraction due to cement production at the Global Atmosphere Watch (GAW) program of the World Meteorological Organization (WMO) stations. In

55 this context, simultaneous observations of $\delta(O_2/N_2)$ and CO_2 amount fractions are expected to be useful for separating out the cement production signal owing to its characteristic ER value. Moreover, Keeling et al. (2011), who examined the possibility of verifying rates of carbon capture and storage (CCS) and direct air capture of CO_2 (DAC) by using changes in the atmospheric constituents, suggested that combined measurements of the $\delta(O_2/N_2)$ and CO_2 could powerfully constrain estimated rates.

    To investigate CO_2 leak detection from a CCS site, van Leeuwen and Meijer (2015) observed $\delta(O_2/N_2)$ and CO_2 from a

60 6-m-tall mast that was 5–15 m away from artificial CO_2 release points. They estimated that their measurement system could detect a CO_2 leak of 10^3 t a^{-1} at a location up to 500 m away from the leak point. Pak et al. (2016) monitored the air for CO_2 plumes at locations between 1 and 100 m from an artificial CO_2 release point, and collected air samples typically between 9 and 20 m from the point where the CO_2 amount fraction was 100–600 $\mu mol\ mol^{-1}$ above ambient. They then analysed the air samples for O_2 and CO_2 amount fractions and found much lower ERs than those expected from fossil fuel combustion and

65 terrestrial biospheric activities. These studies support the suggestion by Keeling et al. (2011) regarding the usefulness of $\delta(O_2/N_2)$ and CO_2 measurements. As the next step to verify the usefulness of combined measurements of $\delta(O_2/N_2)$ and CO_2, their applicability to the detection of not only CO_2 leaks but also CO_2 capture from flue gas should be examined. In this regard,

CCS/DAC plants remove CO_2 from the atmosphere without causing any O_2 changes, just as cement plants do, differing only in the direction of CO_2 exchange between the plant and the atmosphere. Therefore, it should be possible to evaluate the ability
70   of combined measurements to detect a CO_2 capture signal by showing that they can be used to detect a cement production signal.

       In this paper, we present evidence of the successful detection of a cement production signal by combined measurements of $\delta(O_2/N_2)$ and CO_2 at a ground station (a designated WMO/GAW local site) located near a cement plant. We also examine the usefulness of the measurements for future detection of CCS/DAC signals by using a fine-scale 3-D atmospheric transport
75   model to investigate the consistency between the observed signal and the simulated CO_2 emissions from the plant.

2 Methods

2.1 Observations of atmospheric δ(O₂/N₂) and CO₂ amount fractions

       Atmospheric $\delta(O_2/N_2)$ and CO_2 amount fractions have been observed continuously at a coastal station Ryori (RYO: 39° 2′ N, 141° 49′ E, 260 m a.s.l.; Fig. 1), Japan, since 2017, by using a paramagnetic O_2 analyzer (POM-6E, Japan Air Liquid)
80   and a non-dispersive infrared CO_2 analyzer (NDIR; LI-7000, LI-COR), respectively. RYO is a designated WMO/GAW station, and the Japan Meteorological Agency (JMA) has also observed CO_2, CH_4, and CO amount fractions there since 1987, 1991, and 1991, respectively (e.g. Wada et al., 2011). The CO_2, CH_4, and CO amount fraction data observed by JMA are available online at the WMO World Data Centre for Greenhouse Gases (WMO/WDCGG; https://gaw.kishou.go.jp/). A cement plant (Taiheiyo Cement Ofunato plant) is 6 km away from RYO (Fig. 1). It should be noted that the CO_2 amount fraction data posted
85   on WDCGG have already been classified into the data for background air and those affected by local fossil fuel combustion including the cement production discussed in this study. The annual cement production at the plant is 1.966×10^6 t a^{-1} (https://www.taiheiyo-cement.co.jp/english/index.html).

       The $\delta(O_2/N_2)$ is reported in per meg, where 1 per meg is 0.001 ‰:

$$90 \quad \delta(O_2/N_2) = \frac{R_{\text{sample}}\left(^{16}O^{16}O / ^{14}N^{14}N\right)}{R_{\text{standard}}\left(^{16}O^{16}O / ^{14}N^{14}N\right)} - 1, \tag{2}$$

where the subscripts "sample" and "standard" indicate the sample air and the standard gas, respectively. Because O_2 amount fraction in dry air is 0.2093 to 0.2094 mol mol^{-1} (Tohjima et al., 2005; Aoki et al., 2019), the addition of 1 μmol of O_2 to 1 mol of dry air increases $\delta(O_2/N_2)$ by 4.8 per meg (= 1/0.2094). If CO_2 is converted one-for-one into O_2, it causes $\delta(O_2/N_2)$ to
95   increase by 4.8 per meg, which is equivalent to an increase of 1 μmol mol^{-1} of O_2 for each 1 μmol mol^{-1} decrease in CO_2. Therefore, observed relative changes in $\delta(O_2/N_2)$ were converted to those in O_2 amount fraction by multiplying by 0.2094 μmol mol^{-1} (per meg)$^{-1}$.

In this study, $\delta(O_2/N_2)$ of each air sample was measured with a paramagnetic analyzer using high- and low-span standard air of which $\delta(O_2/N_2)$ had been measured against our primary standard air (Cylinder No. CRC00045; AIST-scale) using a mass spectrometer (Thermo Scientific Delta-V) (Ishidoya and Murayama, 2014). The scale based on the primary standard air is our original scale, called as "EMRI/AIST scale" in Aoki et al. (2021). Sample air was taken at the tower heights of 20 m using a diaphragm pump at a flow rate higher than 10 L min^{-1} to prevent thermally-diffusive fractionation of air molecules at the air intake (Blaine et al., 2006). The tower situates on the windward side of prevailing wind direction, and the surface below the tower consists of short grass. Then, a large portion of the air is exhausted from the buffer, with the remaining air allowed to flow into the analyzers from the center of the buffer. It is then sent to an electric cooling unit with a water trap cooled to −80°C at a flow rate of 100 mL min^{-1}, with the pressure stabilized to 0.1 Pa and measured for 90 minutes. After the measurements, high-span standard gas, prepared by adding appropriate amounts of pure O_2 or N_2 to industrially prepared CO_2 standard air, was introduced into the analyzers with the same flow rate and pressure as the sample air and measured for 5 minutes, and then low-span standard gas was measured by the same procedure. The dilution effects on the O_2 mole fraction measured by the paramagnetic analyzer were corrected experimentally, not only for the changes in CO_2 of the sample air or standard gas measured by the NDIR, but also for the changes in Ar of the standard gas measured by the mass spectrometer as $\delta(Ar/N_2)$.

The analytical reproducibility of the $\delta(O_2/N_2)$ and CO_2 amount fraction measurements by the system was determined by repeated measurements of standard gas and found to be about 5 per meg and 0.06 µmol mol^{-1}, respectively, for 2-minute-average values. For more information see Ishidoya et al. (2017). In this study, we use about 70-minute-average mean values for analysis. It should be noted that gaps in the data seen at the end of August to beginning of September 2017 are due to maintenance and technical issues other than routine calibrations described above. The number of $\delta(O_2/N_2)$ (and CO_2 amount fraction) data points shown in Fig. 2 is 9221. Note that we used a mass spectrometer to measure both $\delta(O_2/N_2)$ and the CO_2 amount fraction of the working standard air, whereas we determined the CO_2 amount fraction on the TU-10 scale using a gravimetrically prepared air-based CO_2 standard gas system (Nakazawa et al., 1997). However, we found that the CO_2 amount fractions observed in this study were systematically higher by about 1 µmol mol^{-1} than those observed by JMA and reported on the WMO scale (X2007), which is larger than that expected from the scale difference of about 0.2 µmol mol^{-1} between the TU-10 and WMO scales (Tsuboi et al., 2016). This discrepancy might be related to the LI-7000 NDIR used in this study because no significant difference has been found between the TU-10 and WMO scales at Minamitorishima, where a different NDIR (LI-820, LI-COR) has been used for continuous measurements of $\delta(O_2/N_2)$ and CO_2 amount fractions (Ishidoya et al., 2017). However, we found no significant difference in span sensitivities between the CO_2 amount fractions observed in this study and those observed by JMA. Therefore, the systematic difference between the observed CO_2 amount fractions and those observed by JMA does not affect the ER values, discussed in section 3, which were calculated from changes in O_2 and CO_2 amount fractions.

2.2 Simulation of atmospheric CO_2 and O_2 amount fractions using an atmospheric transport model

130   To calculate local transport of CO_2 around RYO, we used the National Institute of Advanced Industrial Science and Technology (AIST) Mesoscale Model (AIST-MM) fine-scale regional atmospheric transport model (Kondo et al., 2001). AIST-MM is a one-way nested model with an outer domain that covers East Japan with an approximately 10-km grid interval and an inner domain that covers an area of 120 km by 120 km near Ryori with a grid interval of approximately 1 km (Fig. 1). The EAGrid2010-Japan emissions inventory (Fukui et al., 2014), an update of the EAGrid2000-Japan inventory (Kannari et

135   al., 2007) to the year 2010, was used for fossil fuel combustion. In this study, fossil fuel combustion means anthropogenic CO_2 sources other than cement production. Spatial resolution of EAGrid2010-Japan is approximately 1 km, and temporal resolution is monthly average of 1 hour. No further inter-annual correction of emissions is employed, but EAGrid2010-Japan considers the difference in traffic volume between weekdays and holidays. To calculate the CO_2 budget for vegetation, the NCAR Land Surface Model (Bonan, 1996) was used as a sub-model, replacing the simple function of temperature and solar insolation used

140   in the original AIST-MM for this calculation. The cement plant source was set at the location of the plant's stack, at the effective stack height of 275 m. The CO_2 emissions from the cement plant were estimated from the clinker production capacity of the Ofunato plant in 2018 (Japan Cement Association 2020). The clinker is a solid material produced in the cement manufacture as an intermediary product of Portland cement, mainly consisting of CaO, SiO_2, Al_2O_3 and Fe_2O_3. The annual emissions were calculated using the method of the Ministry of Environmental Protection (https://www.env.go.jp/earth/ondanka/ghg-

145   mrv/methodology/material/methodology_2A1.pdf, in Japanese) as

$$E = P \times F \times D, \tag{3}$$

where E is the annual emissions of CO_2 from the cement plant (t a^{-1}), P were the annual production capacity of clinker at the cement plant (t a^{-1}), F is the CO_2-to-clinker mass ratio of 0.516, and D is the cement kiln dust of 1. For initial and boundary conditions, we used GPV/MSM (grid point value of meso-scale model) meteorological data of wind, temperature, and humidity

150   from JMA (https://www.jma.go.jp/jma/en/Activities/nwp.html). As a result, CO_2 amount fractions at RYO are calculated by summing up the contributions of CO_2 amount fraction for fossil fuel combustion, terrestrial biospheric activities, and cement production. In this study, not only CO_2 amount fractions but also ER are compared between the observed and simulated data. For this purpose, O_2 amount fractions are calculated by summing up the respective contributions of CO_2 amount fractions for fossil fuel combustion, terrestrial biospheric activities, and cement production multiplied by the –ER values of –1.4, –1.1, and

155   0. Here the 1.4 and 1.1 are typical ER for fossil fuel combustion and terrestrial biospheric activities, respectively. For comparison, we also calculate ER values for the O_2 and CO_2 amount fractions simulated without including the contribution of cement production. In this regard, it should be noted that Faassen et al. (2023) carried out continuous observations of $\delta(O_2/N_2)$ and the CO_2 amount fraction at a forest site in Finland, and they found higher ER (referred to as "ER$_{atmos}$" in their study) than 2.0 during the morning transition for the average diurnal cycle in summer. Such high ER cannot be obtained from summing

160   up the contributions of fossil fuel combustion and terrestrial biospheric activities at the surface, so that they suggested the ER signal not only represented the diurnal cycle of the forest exchange but also includes other factors, including entrainment of

書式を変更: (言語 1) 日本語, (言語 2) 英語 (米国)

削除:

air masses in the atmospheric boundary layer before midday, with different thermodynamic and atmospheric composition characteristics. Considering their results, we examined average diurnal cycles of $\delta(O_2/N_2)$ and the CO_2 amount fraction at RYO in October 2017 and August 2018 (Fig. A1a-d in Appendix A). We found the ER values are close to 1 throughout the day both for the observed and simulated diurnal cycles. Therefore, we consider the entrainment of air masses do not change the ER at RYO substantially, and the atmospheric transport processes in the AIST-MM is appropriate to compare the observational results in the present study.

2.3 Extraction of a cement signal from the observed data

We extract signals of cement production based on the simultaneous measurements of $\delta(O_2/N_2)$ and CO_2 amount fractions. For this purpose, we use $y(CO_2^*)$ as an indicator:

$$y(CO_2^*) = y(CO_2) + \frac{X(O_2)}{\alpha_{B+F}}\delta(O_2/N_2), \tag{4}$$

where $X(O_2)$ (= 0.2094) is the fraction of atmospheric O_2, and α_{B+F} is the expected ER for terrestrial biospheric activities and fossil fuel combustion. The $y(CO_2^*)$ is closely related to atmospheric potential oxygen ($\delta(APO)$), which is conserved for terrestrial biospheric activities (Stephens et al., 1998). Here, y stands for the dry amount fraction of gas, as recommended by the IUPAC Green Book (Cohen et al., 2007). In our previous study, we calculated $\delta(APO)$ as:

$$\delta(APO) = \delta(O_2/N_2) + \frac{\alpha_B}{X(O_2)}y(CO_2) - 2000 \times 10^{-6}, \tag{5}$$

where 2000 is an arbitrary reference (Ishidoya et al., 2022). For α_{B+F} values, we use monthly average ER values calculated from the simulated O_2 and CO_2 values without considering the contribution of cement production (black dotted line in Fig. 5, bottom, discussed below). If there are no substantial contributions from air–sea O_2 and CO_2 exchanges, then $y(CO_2^*)$ indicates the change in the atmospheric CO_2 amount fraction due only to cement production. No air–sea exchanges can be assumed if the wind field, surface ocean biological production and ocean temperature are constant throughout the month. Actually, day-to-day variations in $\delta(O_2/N_2)$ due to the contribution of oceanic signal cannot be ignorable within a month as reported by past studies (e.g. Goto et al., 2017). However, as discussed in Figs. 5 and 6 below, variations in CO_2 amount fraction due to cement production occurred over periods of less than a day. Taking these findings into consideration, we derived the baseline variation in $y(CO_2^*)$, which does not include a substantial contribution from cement production, as follows. First, we calculated the standard deviation (1σ) of each $y(CO_2^*)$ value from the 24-h running means of $y(CO_2^*)$. Then, we removed $y(CO_2^*)$ values greater than the 24-h running mean of $y(CO_2^*)$ + 1σ from the analysis. Finally, we recalculated the 24-h running means by using the residual $y(CO_2^*)$ values, and regarded them as the baseline variation. Accordingly, the $y(CO_2^*)$ anomaly obtained by subtracting the baseline variation from each $y(CO_2^*)$ value is considered to indicate CO_2 changes due mainly to the contribution of the cement production.

3 Results and discussion

From August 2017 to November 2018, $\delta(O_2/N_2)$ and CO_2 amount fractions observed at RYO varied cyclically in opposite
phase to each other on timescales from several hours to seasonal (Fig. 2); however, variations in CO_2 and CO amount fractions
were roughly in phase. The opposite-phase variations of $\delta(O_2/N_2)$ and CO_2 amount fractions were driven by fossil fuel
combustion and terrestrial biospheric activities. In contrast, the atmospheric O_2 variation ($\mu mol\ mol^{-1}$) due to the air–sea
exchange of O_2 is much larger than that of CO_2 on timescales shorter than 1 year because of the difference in their equilibration
times between the atmosphere and the surface ocean: the equilibration time for O_2 is about a month and CO_2 is about a year
because of the carbonate dissociation effect on the air–sea exchange of CO_2 (Keeling et al., 1993). The in-phase variations of
the CO_2 and CO amount fractions were also driven by fossil fuel combustion and biomass burning. $CO:CO_2$ ratios for fossil
fuel combustion and biomass burning reported by past studies are about 0.01-0.04 and >0.1, respectively (e.g. Nara et al.,
2011; Tohjima et al., 2014; Niwa et al., 2014). The short-term (several hours to several days) variations in $CO:CO_2$ ratios were
about 0.01 from late autumn to early spring, but they were much smaller in summer (Fig. 2). These results suggest, therefore,
that the short-term variations in $\delta(O_2/N_2)$ and CO_2 amount fractions were driven mainly by fossil fuel combustion in winter
and mainly by terrestrial biospheric activities in summer. Over one year of measurements CO amount fractions also showed a
seasonal cycle with a summertime minimum that is attributed to the air mass around Japan: in winter the air mass is of
continental origin and in summer it is of maritime origin.

In this study, we focused on the short-term variations in $\delta(O_2/N_2)$ and the CO_2 and CO amount fractions (Fig. 2) to
extract local effects of cement production. Therefore, we subtracted 1-week rolling average values of $\delta(O_2/N_2)$ and the CO_2
and CO amount fractions from the observed values to exclude their baseline variations, and examined the relationships among
the residuals ($\Delta y(O_2)$, $\Delta y(CO_2)$, and $\Delta y(CO)$; Fig. 3a). Here, $\Delta y(O_2)$ is the equivalent value in $\mu mol\ mol^{-1}$ converted from
$\delta(O_2/N_2)$. We also plotted the ER values calculated by least-squares fitting of regression lines to the observed $\Delta y(O_2)$ and
$\Delta y(CO_2)$ values during successive 24-h periods in Fig. 3b. As seen in the figure, both ER values higher and lower than 1.1
were observed throughout the observation periods. When terrestrial biosphere emits CO_2 to the atmosphere, i.e. respiration
signal is larger than photosynthesis signal, the ER values ranging from 1.05 to 2.00 are expected from combination fluxes of
terrestrial biospheric activities, gas, liquid, and solid fuels combustion. Similar ER values have been observed at other Japanese
sites (e.g. Minejima et al., 2012; Goto et al., 2013; Ishidoya et al., 2020).

On the other hand, when photosynthesis signal is larger than respiration signal, ER for the combination fluxes could be
variable and potentially even become lower than 1.05. Therefore, we consider the observed low ER values with high $\Delta y(CO)$
and $\Delta y(CO_2)$ are attributed to substantial CO_2 flux from cement production, of which ER value is 0, rather than the
photosynthesis signal. These characteristics can be seen from the typical ER, $\Delta y(CO)$ and $\Delta y(CO_2)$ in August 2018 plotted in
Fig. 3c. Therefore, it is considered that the air mass having ER lower than 1.05 and $\Delta y(CO)$ and $\Delta y(CO_2)$ higher than 0
simultaneously indicates CO_2 flux from cement production mixes with the surrounding air that has already been influenced by
terrestrial biospheric activities or fossil fuels combustion. Similar characteristic relationships have previously been observed

削除: However

削除:

書式を変更: 下付き

削除: because the low ER values and high $\Delta y(CO)$ appeared simultaneously…

削除: and

削除: the

削除: lower than 1.05

only in artificial CO_2 release experiments of which ER value is 0, such as those described by van Leeuwen and Meijer (2015) and Pak et al. (2016). Therefore, we used the AIST-MM model to calculate atmospheric CO_2 amount fractions, with or without

235 taking into account the CO_2 flux from the cement plant near RYO, and to convert the calculated CO_2 amount fractions to O_2 amount fractions using the respective ER values of fossil fuels and terrestrial biospheric activities. Then we compared the observed and simulated ER values. Figure 4 shows examples of the performance of the AIST-MM at the present calculation. Figure 4a shows monthly average of hourly CO_2 amount fraction is slightly overestimated at night and underestimated in the daytime except for February, however, absolute value of the difference is less than 2 $\mu mol\ mol^{-1}$ in most case. Figure 4b is a

240 scatter plot of the difference from 391.14 $\mu mol\ mol^{-1}$ (the minimum concentration of observed CO_2 in the 7-months) between calculated and observed concentration for all the hourly data in the 7-months. FAC2 (fraction of calculations within a factor 2 of observations) is 0.976, where model acceptance criterion of FAC2 is greater than 0.5 (Hanna and Chang, 2012), and Pearson's correlation coefficient is 0.69. The discrepancies between observed and simulated values can be attributed to the limited resolution of the model in the complex terrain, or to problems in the parameterization of transport processes, or in the

245 CO_2 sources/sinks incorporated into the AIST-MM.

In October 2017, short-term variations in observed CO_2 and $\delta(O_2/N_2)$ were opposite in phase, and the amplitudes (in $\mu mol\ mol^{-1}$) of some CO_2 variations were larger than those of the corresponding $\delta(O_2/N_2)$ variations (Fig. 5). If the short-term variations were driven by terrestrial biospheric activities and the consumption of gas, liquid, and solid fuels, then the amplitudes of CO_2 should be smaller than those of the $\delta(O_2/N_2)$. Therefore, this result suggests an effect of cement production

250 superimposes on fossil fuel combustion and/or terrestrial biospheric activities. Similar characteristic variations suggesting a cement production effect were also seen in the observations made at RYO in November 2017 and in January, February, April, May, and August 2018 as presented in Appendix B. The simulated CO_2 amount fraction, calculated from the sources and sinks in East Japan area with no background amount fraction by the AIST-MM, is also shown in Fig. 5. The contribution of CO_2 amount fraction for the three components (cement production, terrestrial biospheric activities, and fossil fuel consumption

255 other than cement production) are also shown in Fig. 5. The results demonstrate that cement production contributed substantially to the simulated CO_2 amount fraction. We examined the effect of cement production on ER values by calculating ER values by fitting regression lines to the observed and simulated O_2 and CO_2 amount fractions during successive 24-h periods (Fig. 5, bottom). Both the observed ER values and those simulated are frequently lower than 1.1, while the ER values simulated without including cement production show lower values than 1.1 occasionally (Fig. 5 and Fig. B1a-f in Appendix B). Therefore,

260 CO_2 emissions from the cement plant must be incorporated into the transport model to reproduce the detailed variations in atmospheric O_2 and CO_2 amount fractions at RYO.

Next, we extracted signals of cement production based on $y(CO_2^*)$ calculated from the simultaneous measurements of $\delta(O_2/N_2)$ and CO_2 amount fractions (see details in section 2.3). In October 2017, $y(CO_2^*)$ and CO amount fraction maxima at RYO appeared at the same time that the wind was blowing from the northwest (most frequently over the range of 270-300°)

265 (https://www.data.jma.go.jp/env/data/report/data/download/atm_bg_e.html) (Fig. 6). This result suggests that the short-term

削除: seven

削除: A

削除: A

削除: A

削除: 2.3 in

variations in $y(CO_2^*)$ were driven mainly by air masses transported from the cement plant, which is about 6 km northwest of RYO. These findings also indicate that it is possible to extract CO_2 amount fraction data from background air at RYO by selecting observed ER and CO amount fraction data. We have confirmed the present method of JMA used to select background air for the data posted on WDCGG is sufficient to exclude the effect of cement production, nevertheless the use of ER may

275 provide an additional constraint. Note that CO is emitted during fossil fuel combustion at the cement plant to supply electricity and heat for cement production. This means CO_2 is presumably released as well, so that the overall ER for the CO_2 emitted from cement plant (cement production + fossil fuel combustion) would not be 0.

To examine the consistency between the observed $y(CO_2^*)$ and simulated CO_2 emissions from the cement plant, we compared 5-h means of $y(CO_2^*)$ anomalies with changes in the CO_2 amount fraction due to the contribution of cement

280 production as simulated by the AIST-MM (hereafter referred to as "$y(CO_2, cement)$") (Fig. 6, bottom). The result shows that variations in the $y(CO_2^*)$ anomaly and $y(CO_2, cement)$ are of the same order of magnitude, although they do not necessarily occur simultaneously. This result suggests that we succeeded in using $y(CO_2^*)$ to detect a signal of CO_2 emissions owing to the cement production, and that this signal can be used to validate a fine-scale atmospheric transport model. In this context, van Leeuwen and Meijer (2015) suggested that a CO_2 leak of 10^3 t a^{-1} is detectable at a location up to 500 m away from the

285 leak point based on their observations of atmospheric O_2 and CO_2 amount fractions. If this relationship follows an inverse square law, a CO_2 leak of 1.44×10^5 t a^{-1} should be detectable at locations up to 6 km from the leak point. Therefore, about 10^6 t a^{-1} of the CO_2 emissions from the cement plant in this study, calculated with Eq. (3), is large enough to be detected at RYO. Features during November 2017, January, February, April, May and August 2018 were similar (Fig. B2a-f in Appendix B), although the short-term variations in $y(CO_2^*)$ in May 2018 (Fig. B2e) were noisier than in the other months, probably

290 because of an effect of short-term variations in the air–sea O_2 flux due to high primary production during the spring bloom in the nearby coastal ocean (e.g. Yamagishi et al., 2008).

The monthly mean $y(CO_2^*)$ anomalies shown in Fig. 7 were calculated using the ER (α_{B+F}) value calculated by the AIST-MM for terrestrial biospheric activities and fossil fuel consumption excluding cement production. In Fig. 7, these $y(CO_2^*)$ anomaly values as well as those calculated using α_{B+F} values of 1.4 and 1.1 are compared with monthly mean $y(CO_2, cement)$

295 values. The monthly mean $y(CO_2^*)$ anomalies were generally consistent with the monthly mean $y(CO_2, cement)$ values from October, November, February and April, while those were smaller in January and larger in May and August. The discrepancy between the monthly mean $y(CO_2^*)$ anomaly and $y(CO_2, cement)$ is not explained by month-to-month changes in the cement production, since the production of clinker at the cement plant for each month was not markedly different with each other (personal communication with Taiheiyo Cement Co.). We have also confirmed monthly mean $y(CO_2, cement)$ values were

300 related to the occurrence of northwesterly winds (i.e. wind blowing from the cement plant). However, the average wind direction simulated by the AIST-MM when high $y(CO_2, cement)$ values appeared (around 300°) was slightly but systematically different from that for observed wind direction (around 270°) (Fig. B3a and B3b in Appendix B). This discrepancy is probably due to the underestimation of the altitude of Ryori ridge which is located between the cement plant and the RYO site. Such the underestimation makes it easy to transport the CO_2 emitted from the cement plant directly to RYO over the ridge since the

cement plant is located around 300° from the RYO site. This is also consistent with the fact that the larger monthly mean $y(CO_2, cement)$ than the monthly mean $y(CO_2^*)$ anomalies are found in January and February when prevailing wind direction is northwesterly. The complex terrain around RYO such as Ryori ridge would also contribute to the discrepancy between the monthly mean $y(CO_2^*)$ anomaly and $y(CO_2, cement)$ in May and August at least partly. In May, it is considered that an effect of the oceanic O_2 flux on $y(CO_2^*)$ anomaly is also substantial, since we can distinguish short-term variations in $\delta(O_2/N_2)$ without simultaneous changes in CO_2 amount fraction (Fig. B1e).

It was also found from Fig. 7 that the monthly mean $y(CO_2^*)$ anomaly did not depend on the α_{B+F} value used to calculate $y(CO_2^*)$ except August, 2018. In addition, the average monthly mean $y(CO_2^*)$ anomaly values and the average $y(CO_2, cement)$ during the 7 months (right side of Fig. 7) agreed within their monthly variabilities. These results suggest that it is not necessary to use the α_{B+F} value simulated by the AIST-MM to estimate the contribution of cement production to the atmospheric CO_2 amount fraction at RYO; rather, it can be estimated from only the observed $y(CO_2^*)$ by assuming an α_{B+F} value of 1.1 or 1.4. This is also applicable on shorter time scales (Figures B4a and B4b in Appendix B). Therefore, we can derive the observed $y(CO_2^*)$ at RYO is without using any simulated value by an atmospheric transport model, and the observed $y(CO_2^*)$ can be used to validate hourly to annual average CO_2 fluxes from cement production simulated by a fine-scale atmospheric transport model. It should be also noted that we did not use CO amount fraction for the calculation of $y(CO_2^*)$. This is an important advantage to apply $y(CO_2^*)$ to detect CO_2 capture and/or CO_2 leak which do not emit CO.

$y(CO_2^*)$ is expected to be an indicator for detecting the signal of CO_2 capture from the flue gas at the cement plant. At a cement plant, CO_2 is removed from the flue gas without any O_2 changes. Therefore, if the CO_2 emitted during cement production, which is about 10^6 t a^{-1} at this plant, is removed from the flue gas, then the 7-month mean $y(CO_2^*)$ anomaly would change from 0.4 to 0 µmol mol^{-1}. Thus, a cement plant can be a useful site not only for demonstrating carbon capture from flue gas but also for monitoring its efficiency based on combined measurements of $\delta(O_2/N_2)$ and CO_2. In addition, during the future operation of a large-scale DAC plant, a negative annual mean $y(CO_2^*)$ anomaly value should be observed because a DAC plant removes CO_2 from the atmosphere without emitting O_2 to the atmosphere.

4 Conclusions

We analysed atmospheric $\delta(O_2/N_2)$ and CO_2 and CO amount fraction data observed continuously at RYO to extract a CO_2 emissions signal from a cement plant located about 6 km northwest of RYO. The observed $\delta(O_2/N_2)$ and CO_2 amount fractions varied cyclically in opposite phase to each other on timescales from several hours to seasonal. From the CO:CO_2 ratios, the short-term variations in $\delta(O_2/N_2)$ and CO_2 amount fraction were inferred to be driven mainly by fossil fuel combustion in winter and by terrestrial biospheric activities in summer. We found that an ER lower than 1.1 was frequently associated with short-term variations, especially when the CO amount fraction was high; this result suggests a substantial effect of cement production, which has an ER of 0. We compared observed CO_2 amount fractions with those simulated by the AIST-

削除: s

削除: A

削除: monthly

MM for October and November 2017 and January, February, April, May, and August 2018. FAC2 for the data throughout the observation period was 0.976, which was greater than model acceptance criterion of 0.5. Therefore, the AIST-MM reproduced general characteristics of the observed CO_2 amount fraction were reproduced by the AIST-MM.

350   We calculated the simulated ER values by using simulated $\delta(O_2/N_2)$ values obtained from simulated CO_2 amount fractions and ER values of 1.1, 1.4, and 0 for terrestrial biospheric activities, fossil fuel combustion, and cement production, respectively. As in the observations, simulated ER values lower than 1.1 were frequently associated with short-term variations. $y(CO_2^*)$ was calculated from the observed $\delta(O_2/N_2)$ and CO_2 amount fractions and the simulated α_{B+F} to extract the cement production signal. Variations in the $y(CO_2^*)$ anomaly relative to baseline values were generally of the same order of magnitude

355 as CO_2 amount fraction changes due to contribution of cement production simulated by the AIST-MM ($y(CO_2, \text{cement})$). The monthly mean $y(CO_2^*)$ anomaly averaged over the 7 months examined in this study and the 7-month average of $y(CO_2, \text{cement})$ agreed within their variabilities.

      These results confirm that monthly to annual average CO_2 emissions from a cement plant can be detected by using $y(CO_2^*)$, and, therefore, that a cement plant will be a useful site for demonstrating and monitoring CO_2 capture from flue gas

360 in the future. As a remaining topic, some of the more detailed variations in the CO_2 amount fractions were not reproduced by the AIST-MM. This is at least partially due to the spatial resolution of the AIST-MM which limited its ability to reproduce air transport from a point source, such as the cement plant in the present study. In the future this work could be expanded on by using a higher resolution atmospheric transport model to improve the agreement between the observed and simulated CO_2 amount fractions. An additional step could be developing a more accurate method for extracting $y(CO_2^*)$ due only to cement

365 production, especially for the period when air-sea O_2 flux is substantial. This would improve the estimation of the amount of CO_2 capture and/or CO_2 leak around the observation site from an inversion analysis using the higher-resolution atmospheric transport model.

Appendix A: Additional figures to evaluate the effect of entrainment of air mass on the observed ER

370   As we described in 2.2, Faassen et al. (2023) found higher ER ("ER$_{atmos}$" in their study) than 2.0 at a forest site in Finland during the morning transition for the average diurnal cycles of $\delta(O_2/N_2)$ and the CO_2 amount fraction in summer. On the other hand, Ishidoya et al. (2013) reported ER values ("ER$_{atm}$" in their study) close to 1 at a Japanese forest site in summer, for the average diurnal cycles throughout the day. Considering the discrepancy between Faassen et al. (2023) and Ishidoya et al. (2013), we derive the average diurnal cycle of $\delta(O_2/N_2)$ and the CO_2 amount fraction at RYO. For this purpose, deviations of

375 $\delta(O_2/N_2)$ and the CO_2 amount fraction from their 24-hr mean values were calculated, and the $\Delta\delta(O_2/N_2)$ were converted to $\Delta y(O_2)$ by multiplying $X(O_2)$ (=0.2094). Figures A1a-b show the average diurnal cycles of $\Delta y(O_2)$ and $\Delta y(CO_2)$ in October 2017, and their relationship. Those for August 2018 are also shown in Figs. A1c-d. As seen from the figures, the observed $\Delta y(O_2)$ took maxima in the daytime, and the ER values for the average diurnal cycles at RYO were close to 1 throughout the

day. The corresponding diurnal $\Delta y(O_2)$ and $\Delta y(CO_2)$ cycles and their relationships obtained from the simulated results by AIST-MM were also shown in Figs. A1a-d. Similar to the observations, it was found that the simulated $\Delta y(O_2)$ took maxima in the daytime and the ER were close to 1 throughout the day. These facts indicate the observed ER at RYO can be reproduced by the AIST-MM generally, including the period during the morning transition. Therefore, an entrainment of air mass to yield high ER during the morning suggested by Faassen et al. (2023) may be a characteristic phenomenon at their observational site.

Appendix B: Additional figures to evaluate the effect of cement production on the observed and simulated CO$_2$ amount fractions

In the main text, variations in CO$_2$ amount fractions and $\delta(O_2/N_2)$ observed at RYO, CO$_2$ amount fraction simulated by the AIST-MM, and ER calculated from the observed and simulated data in October 2017 were shown in Fig. 5. We also show the corresponding figures in November, 2017, and January, February, April, May, and August, 2018 in Fig. B1a, B1b, B1c, B1d, B1e, and B1f, respectively. Variations in $y(CO_2^*)$, CO amount fractions in October 2017, and five-hour-averages of the $y(CO_2^*)$ anomalies from the $y(CO_2^*)$ baseline variation and those of $y(CO_2, cement)$ simulated by the AIST-MM were shown in Fig. 6. We also show the corresponding figures in November, 2017, and January, February, April, May, and August, 2018 in Fig. B2a, B2b, B2c, B2d, B2e, and B2f, respectively. General characteristics of Fig. B1a-f and B2a-f are found to be similar to those discussed in the main text for Fig. 5 and 6, respectively. However, we can distinguish short-term variations in $\delta(O_2/N_2)$ without simultaneous changes in CO$_2$ amount fraction in May 2018 (Fig. B1e), which may be attributed to substantial oceanic O$_2$ flux due to high primary production during the spring bloom.

Figure B3a shows relationships between $y(CO_2^*)$ and wind direction at RYO. Same as in B3a but for $y(CO_2, cement)$ simulated by the AIST-MM is shown in B3b. The average wind direction when high $y(CO_2, cement)$ values appeared is around 300°, while that for observed wind direction is around 270°. This discrepancy is probably due to insufficient spatial resolution of the AIST-MM as discussed in the main text.

Figures B4a and B4b show the bottom panels of Fig. 6 and A2a, respectively, but for adding the $\Delta y(CO_2^*)$ calculated by using the α_{B+F} values of 1.4 and 1.1. As seen from the figures, several hours to day-to-day variations in the $\Delta y(CO_2^*)$ did not change substantially depending on the α_{B+F} value used to calculate $y(CO_2^*)$. Therefore, the contribution of cement production to the atmospheric CO$_2$ amount fraction at RYO can be estimated from the observed $y(CO_2^*)$ by assuming an α_{B+F} value of 1.1 or 1.4, not only for monthly time scale but for shorter (hourly to day-to-day) time scale.

Data availability.

The $\delta(O_2/N_2)$ and CO$_2$ amount fraction data at RYO site presented in this study are included as electronic supplement to the manuscript. We will deposit the data in the WDCGG before the manuscript is accepted for publication, and the URL and DOI will be shown here.

Author contributions.

SI designed the study and drafted the manuscript. Measurements of O_2 and CO_2 amount fractions were conducted by SI, KT, and KS. KH conducted the AIST-MM simulations. NA prepared the standard gas for the O_2 measurements. KI and HM examined the results and provided feedback on the manuscript. All authors approved the final manuscript.

Competing interests.

The authors declare that they have no conflict of interest.

Acknowledgements.

We acknowledge the many staff members of the Japan Meteorological Agency. We also thank Shohei Murayama at the National Institute of Advanced Industrial Science and Technology (AIST), Ryo Fujita at the Meteorological Research Institute, and JANS Co. Ltd. For supporting the observations.

Financial support.

This study was partly supported by JSPS KAKENHI (grant nos. 19H01975 and 22H05006) and the Global Environment Research Coordination System from the Ministry of the Environment, Japan (grant nos. METI1454 and METI1953).

References

Aoki, N., Ishidoya, S., Matsumoto, N., Watanabe, T., Shimosaka, T., and Murayama, S.: Preparation of primary standard mixtures for atmospheric oxygen measurements with less than 1 μmol mol^{-1} uncertainty for oxygen molar fractions, Atmos. Meas. Tech., 12, 2631–2646, https://doi.org/10.5194/amt-12-2631-2019, 2019.

Aoki, N., Ishidoya, S., Tohjima, Y., Morimoto, S., Keeling, R. F., Cox, A., Takebayashi, S., and Murayama, S.: Intercomparison of O_2/N_2 ratio scales among AIST, NIES, TU, and SIO based on a round-robin exercise using gravimetric standard mixtures, Atmos. Meas. Tech., 14, 6181–6193, https://doi.org/10.5194/amt-14-6181-2021, 2021.

Bonan, G. B.: A Land surface model (LSM version 1.0) for ecological, hydrological, and atmospheric studies: Technical description and user's guide, Climate and global dynamics division, National Center for Atmospheric Research, Boulder, Colorado, 150 pp., 1996.

Cohen, E. R., Cvitas, T., Frey, J. G., Holmstrom, B., Kuchitsu, K., Marquardt, R., Mills, I., Pavese, F., Quack, M., Stohner, J., Strauss, H., Takami, M., and Thor, A. J.: IUPAC Green Book: 3rd edn., RSC Publishing, ISBN 0854044337, ISBN-13 9780854044337, 2007.

Faassen, K. A. P., Nguyen, L. N. T., Broekema, E. R., Kers, B. A. M., Mammarella, I., Vesala, T., Pickers, P. A., Manning, A. C., Vilà-Guerau de Arellano, J., Meijer, H. A. J., Peters, W., and Luijkx, I. T.: Diurnal variability of atmospheric O_2, CO_2, and their exchange ratio above a boreal forest in southern Finland, Atmos. Chem. Phys., 23, 851–876, https://doi.org/10.5194/acp-23-851-2023, 2023.

480 Friedlingstein, P., O'Sullivan, M., Jones, M. W., Andrew, R. M., Gregor, L., Hauck, J., Le Quéré, C., Luijkx, I. T., Olsen, A., Peters, G. P., Peters, W., Pongratz, J., Schwingshackl, C., Sitch, S., Canadell, J. G., Ciais, P., Jackson, R. B., Alin, S. R., Alkama, R., Arneth, A., Arora, V. K., Bates, N. R., Becker, M., Bellouin, N., Bittig, H. C., Bopp, L., Chevallier, F., Chini, L. P., Cronin, M., Evans, W., Falk, S., Feely, R. A., Gasser, T., Gehlen, M., Gkritzalis, T., Gloege, L., Grassi, G., Gruber, N., Gürses, Ö., Harris, I., Hefner, M., Houghton, R. A., Hurtt, G. C., Iida, Y., Ilyina, T., Jain, A. K., Jersild, A., Kadono, 485 K., Kato, E., Kennedy, D., Klein Goldewijk, K., Knauer, J., Korsbakken, J. I., Landschützer, P., Lefèvre, N., Lindsay, K., Liu, J., Liu, Z., Marland, G., Mayot, N., McGrath, M. J., Metzl, N., Monacci, N. M., Munro, D. R., Nakaoka, S.-I., Niwa, Y., O'Brien, K., Ono, T., Palmer, P. I., Pan, N., Pierrot, D., Pocock, K., Poulter, B., Resplandy, L., Robertson, E., Rödenbeck, C., Rodriguez, C., Rosan, T. M., Schwinger, J., Séférian, R., Shutler, J. D., Skjelvan, I., Steinhoff, T., Sun, Q., Sutton, A. J., Sweeney, C., Takao, S., Tanhua, T., Tans, P. P., Tian, X., Tian, H., Tilbrook, B., Tsujino, H., Tubiello, 490 F., van der Werf, G. R., Walker, A. P., Wanninkhof, R., Whitehead, C., Willstrand Wranne, A., Wright, R., Yuan, W., Yue, C., Yue, X., Zaehle, S., Zeng, J., and Zheng, B.: Global Carbon Budget 2022, Earth Syst. Sci. Data, 14, 4811–4900, https://doi.org/10.5194/essd-14-4811-2022, 2022.

Fukui, T., Kokuryo, K., Baba, T., Kannari, A.: Updating EAGrid2000-Japan emissions inventory based on the recent emission trends, J. Jpn. Soc. Atmos. Environ. 49 (2), 117-125, 2014 (in Japanese).

495 Goto, D., Morimoto, S., Ishidoya, S., Ogi, A., Aoki, S., and Nakazawa, T.: Development of a high precision continuous measurement system for the atmospheric O_2/N_2 ratio and its application at Aobayama, Sendai, Japan, J. Meteorol. Soc. Jpn., 91, 179–192, 2013.

Goto, D., Morimoto, S., Aoki, S., Patra, P. K., and Nakazawa, T.: Seasonal and short-term variations in atmospheric potential oxygen at Ny-Ålesund, Svalbard, Tellus 69B, 1311767, DOI: 10.1080/16000889.2017.1311767, 2017.

500 Hanna, S. R., and Chang, J. C.: Acceptance criteria for urban dispersion model evaluation, Meteorol. Atmos. Phys., 116, 133-146, 2012.

Ishidoya, S., and Murayama, S.: Development of high precision continuous measuring system of the atmospheric O_2/N_2 and Ar/N_2 ratios and its application to the observation in Tsukuba, Japan, Tellus B, 66, 22574, http://dx.doi.org/10.3402/tellusb.v66.22574, 2014.

505 Ishidoya, S., Tsuboi, K., Murayama, S., Matsueda, H., Aoki, N., Shimosaka, T., Kondo, H., and Saito, K.: Development of a continuous measurement system for atmospheric O_2/N_2 ratio using a paramagnetic analyzer and its application in Minamitorishima Island, Japan, SOLA, 13, 230-234, 2017.

Ishidoya, S., Sugawara, H., Terao, Y., Kaneyasu, N., Aoki, N., Tsuboi, K., and Kondo, H.: $O_2 : CO_2$ exchange ratio for net turbulent flux observed in an urban area of Tokyo, Japan, and its application to an evaluation of anthropogenic CO_2 emissions, Atmos. Chem. Phys., 20, 5293–5308, https://doi.org/10.5194/acp-20-5293-2020, 2020.

Ishidoya, S., Tsuboi, K., Niwa, Y., Matsueda, H., Murayama, S., Ishijima, K., and Saito, K.: Spatiotemporal variations of the $\delta(O_2/N_2)$, CO_2 and $\delta(APO)$ in the troposphere over the western North Pacific, Atmos. Chem. Phys., 22, 6953–6970, https://doi.org/10.5194/acp-22-6953-2022, 2022.

Japan Cement Association: Handbook of Cement, 2020.

Kannari, A., Tonooka, Y., Baba, T., Murano, K.: Development of multiple-species 1 km×1 km resolution hourly basis emissions inventory for Japan, Atmos. Environ., 41, 3428–3439, 2007.

Keeling, R. F.: Development of an interferometric oxygen analyzer for precise measurement of the atmospheric O_2 mole fraction, *Ph.D. thesis*, Harvard University, Cambridge, 1988.

Keeling, R. F. and Shertz, S. R. 1992. Seasonal and interannual variations in atmospheric oxygen and implications for the global carbon cycle, Nature, 358, 723-727.

Keeling, R. F., Bender, M. L., and Tans, P. P.: What atmospheric oxygen measurements can tell us about the global carbon cycle, Global Biogeochem. Cycles, 7, 37-67, 1993.

Keeling, R. F., Manning, A. C., and Dubey, M. K.: The atmospheric signature of carbon capture and storage, Phil. Trans. R. Soc. A, 369, 2113-2132 doi: 10.1098/rsta.2011.0016, 2011.

Keeling, R. F. and Manning, A. C.: Studies of recent changes in atmospheric O_2 content, in Treatise on Geochemistry, vol. 5, 2nd ed., Elsevier, Amsterdam, 385–404, 2014.

Kondo, H., Saigusa, N., Murayama, S., Yamamoto, S., and Kannari, A.: A numerical simulation of the daily variation of CO_2 in the central part of Japan—summer case—, J. Meteor. Soc. Japan. Ser. II, 79, 11-21, 2001.

Leeuwen, C.V., and Meijer, H.A.J.: Detection of CO_2 leaks from carbon capture and storage sites with combined atmospheric CO_2 and O_2 measurements, Int. J. Greenh. Gas Control, 41, 194–209, 2015.

Liu, X., Huang, J., Wang, L., Lian, X., Li, C., Ding, L., Wei, Y., Chen, S., Wang, Y., Li, S., and Shi, J.: "Urban Respiration" Revealed by Atmospheric O_2 Measurements in an Industrial Metropolis, Environmental Science & Technology, 57(6), 2286-2296, doi: 10.1021/acs.est.2c07583, 2023.

Minejima, C., Kubo, M., Tohjima, Y., Yamagishi, H., Koyama, Y., Maksyutov, S., Kita, K., and Mukai, H.: Analysis of $\Delta O_2/\Delta CO_2$ ratios for the pollution events observed at Hateruma Island, Japan, Atmos. Chem. Phys., 12, 2713–2723, https://doi.org/10.5194/acp-12-2713-2012, 2012.

Nakazawa, T., Sugawara, S., Inoue, G., Machida, T., Mak-shutov, S. and Mukai, H.: Aircraft measurements of the concentrations of CO_2, CH_4, N_2O and CO and the carbon and oxygen isotopic ratios of CO_2 in the troposphere over Russia. J. Geophys. Res. 102, 3843–3859, 1997.

510

515

520

525

530

535

書式を変更: 下付き

540   Nara, H., Tanimoto, H., Nojiri, Y., Mukai, H., Zeng, J., Tohjima, Y., and Machida, T.: CO emissions from biomass burning in South-east Asia in the 2006 El Niño year: shipboard and AIRS satellite observations, Environmental Chemistry 8(2) 213-223 https://doi.org/10.1071/EN10113, 2011.

Niwa, Y., Tsuboi, K., Matsueda, H., Sawa, Y., Machida, T., Nakamura, M., Kawasato, T., Saito, K., Takatsuji, S., Tsuji, K., Nishi, H., Dehara, K., Baba, Y., Kuboike, D., Iwatsubo, S., Ohmori, H., and Hanamiya, Y.: Seasonal Variations of CO_2,

545   CH_4, N_2O and CO in the Mid-troposphere over the Western North Pacific Observed using a C-130H Cargo Air- craft, J. Meteorol. Soc. Japan, 92(1), doi:10.2151/jmsj.2014- 104, 2014.

Pak, N. M., Rempillo, O., Norman, A-L., and & Layzell, D. B.: Early atmospheric detection of carbon dioxide from carbon capture and storage sites, J. Air Waste Manag. Assoc., 66, 739-747, doi: 10.1080/10962247.2016.1176084, 2016.

Pickers, P. A., Manning, A. C., Le Quéré, C., Forster, G. L., Luijkx, I. T., Gerbig, C., Fleming, L. S., Sturges, W. T.: Novel

550   quantification of regional fossil fuel CO_2 reductions during COVID-19 lockdowns using atmospheric oxygen measurements, Science Advances, 8(16), eabl9250, 2022.

Resplandy, L., Keeling, R.F., Eddebbar, Y., Brooks, M., Wang, R., Bopp, L., Long, M. C., Dunne, J. P., Koeve, W., and Oschlies, A.: Quantification of ocean heat uptake from changes in atmospheric O_2 and CO_2 composition, Sci. Rep., 9, 20244, doi:10.1038/s41598-019-56490-z, 2019.

555   Severinghaus, J.: Studies of the terrestrial O_2 and carbon cycles in sand dune gases and in biosphere 2, Ph. D. thesis, Columbia University, New York, 1995.

Stephens, B. B., Keeling, R. F., Heimann, M., Six, K. D., Murnane, R., and Caldeira, K.: Testing global ocean carbon cycle models using measurements of atmospheric O_2 and CO_2 concentration, Global Biogeochem. Cycles, 12, 213–230, 1998.

Sugawara, H., Ishidoya, S., Terao, Y., Takane, Y., Kikegawa, Y., and Nakajima, K.: Anthropogenic CO_2 emissions changes

560   in an urban area of Tokyo, Japan, due to the COVID-19 pandemic: A case study during the state of emergency in April– May 2020. Geophysical Research Letters, 48, e2021GL092600. https://doi. Org/10.1029/2021GL092600, 2021.

Tohjima, Y., Machida, T., Watai, T., Akama, I., Amari, T., and Moriwaki, Y.: Preparation of gravimetric standards for measurements of atmospheric oxygen and reevaluation of atmospheric oxygen concentration, J. Geophys. Res., 110, D1130, 2005.

565   Tohjima, Y., Kubo, M., Minejima, C., Mukai, H., Tanimoto, H., Ganshin, A., Maksyutov, S., Katsumata, K., Machida, T., and Kita, K.: Temporal changes in the emissions of CH_4 and CO from China estimated from CH_4 / CO_2 and CO / CO_2 correlations observed at Hateruma Island, Atmos. Chem. Phys., 14, 1663–1677, https://doi.org/10.5194/acp-14-1663-2014, 2014.

Tsuboi, K., Matsueda, H., Sawa, Y., Niwa, Y., Takahashi, M., Takatsuji, S., Kawasaki, T., Shimosaka, T., Watanabe, T., Kato,

570   K.: Scale and stability of methane standard gas in JMA and comparison with MRI standard gas, Papers in Meteorology and Geophysics, Vol.66, 15-24, 2016.

Wada, A., Matsueda, H., Sawa, Y., Tsuboi, K., and Okubo, S.: Seasonal variation of enhancement ratios of trace gases observed over 10 years in the western North Pacific, Atmos. Environ., 45, 2129–2137, 2011.

Yamagishi, H., Tohjima, Y., Mukai, H., and Sasaoka, K.: Detection of regional scale sea-to-air oxygen emission related to
575   spring bloom near Japan by using in-situ measurements of the atmospheric oxygen/nitrogen ratio, Atmos. Chem. Phys.,
8, 3325–3335, https://doi.org/10.5194/acp-8-3325-2008, 2008.

580

Figure 1: Location of the Ryori site (RYO) and the cement plant on an aerial photograph from Google Earth. The cement plant is about 6 km northwest of RYO. Inner and outer domains of the fine-scale 3-D atmospheric transport model (AIST-MM) used in the
585   present study are also shown.
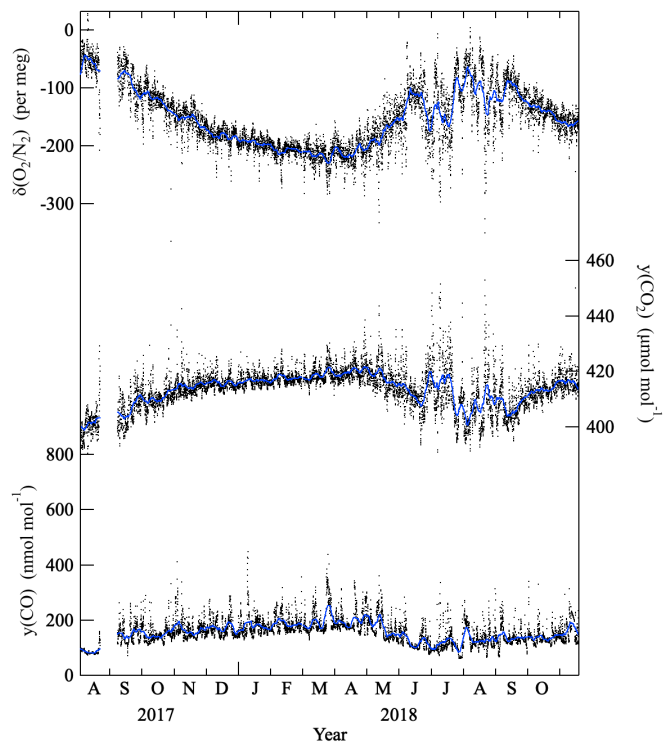
590 **Figure 2:** $\delta(O_2/N_2)$ **and CO₂ and CO amount fractions (black dots) and their 1-week rolling average values (blue lines) observed at Ryori (RYO), Japan, from August 2017 to November 2018.** $\delta(O_2/N_2)$ **and CO₂ y-axes are scaled to be visually comparable.**
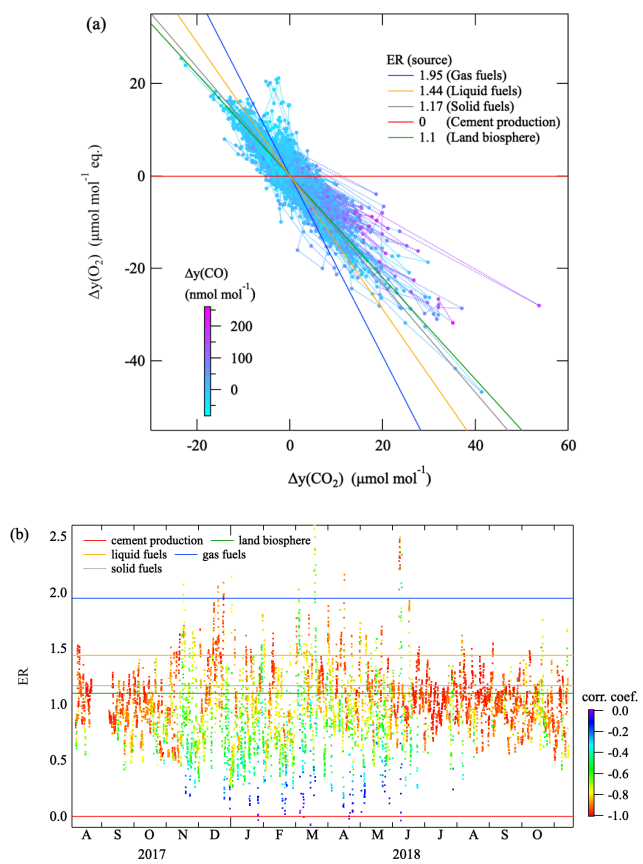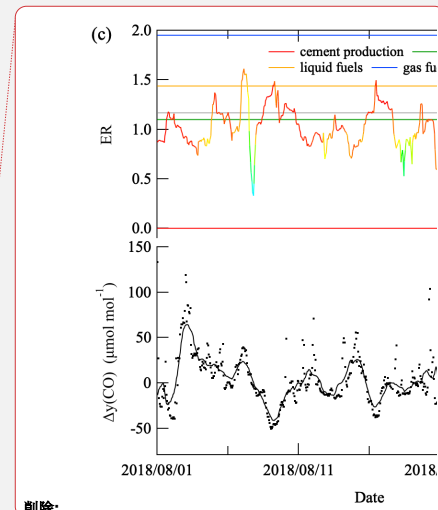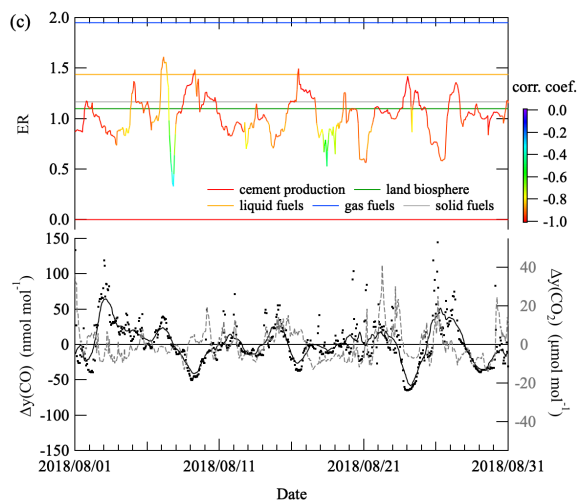
Figure 3: (a) Relationship between $\Delta y(O_2)$ **and** $\Delta y(CO_2)$ **at RYO for the period from August 2017 to November 2018.** $\Delta y(O_2)$**,** $\Delta y(CO_2)$**,**

600 **and** $\Delta y(CO)$ **were calculated by subtracting the 1-week mean values of** $\delta(O_2/N_2)$**,** CO_2 **and CO amount fractions from their observed values; then** $\Delta\delta(O_2/N_2)$ **values were converted to the equivalent** $\Delta y(O_2)$**.** $\Delta y(CO)$ **values are shown by the color scale. The plotted ER values are from Keeling (1988) and Severinghaus (1995). (b) ER values calculated by least-squares fitting of regression lines to the observed** $\Delta y(O_2)$ **and** $\Delta y(CO_2)$ **values shown in (a) during successive 24-h periods (before and after 12-h of each point) throughout the observation period. (c) Same ER as in (b) but for August 2018.** $\Delta y(CO)$ **(black dots) and its 24-h averages (black solid line), and**

605 $\Delta y(CO_2)$ **(gray dashed line) are also shown.**

610 (a)

(b)
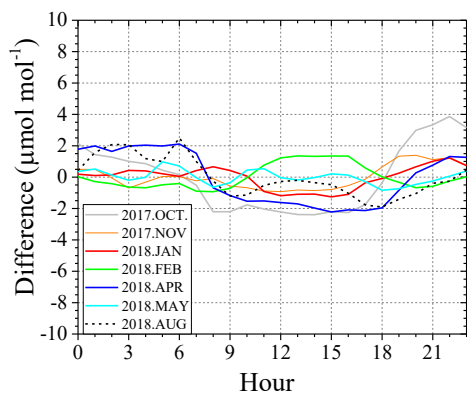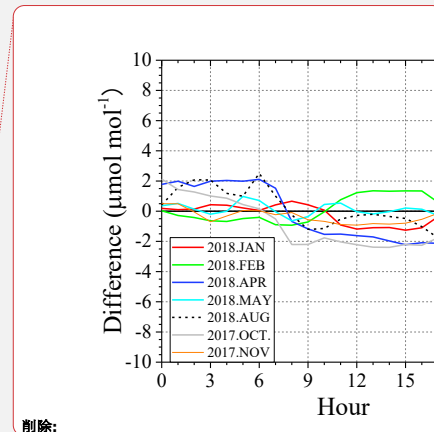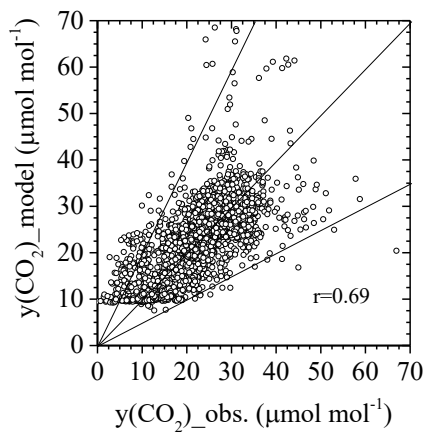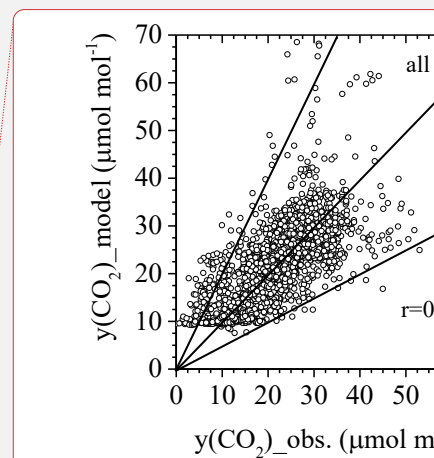
Figure 4: (a) Difference of monthly average of hourly amount fraction of CO_2 between calculated and observed concentration at
615 RYO. (b) Scatter plot between observed and calculated CO_2 amount fraction deviation for all the hourly data of 7 months at RYO.
391.14 μmol mol^{-1} (the minimum value of observed CO_2 amount fraction in 7 months) was subtracted from both of the data
groups. Straight lines indicate the range of FAC2.

書式を変更: フォント：太字

削除:
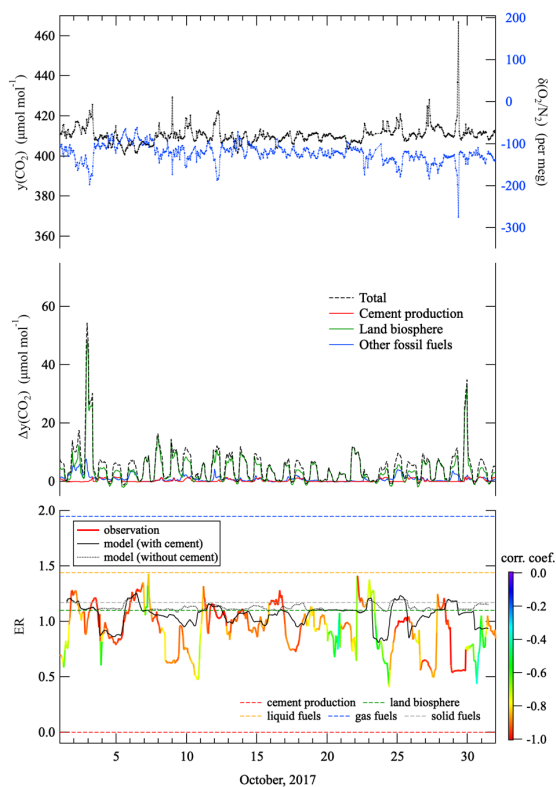
625

Figure 5: (top) Variations in CO_2 amount fractions and $\delta(O_2/N_2)$ observed at RYO in October 2017. (middle) Variations in the total CO_2 amount fraction simulated by the AIST-MM (black dashed line, see text), and the contributions of CO_2 amount fraction for cement production (red solid line), terrestrial biospheric activities (green solid line), and fossil fuel consumption other than cement production (blue solid line). The simulated CO_2 amount fraction were calculated from the sources and sinks in East Japan area with

630   no background amount fraction, i.e. Δ denotes deviations from the background amount fraction. (bottom) Variations in ER calculated by least-squares fitting of regression lines to the observed $\delta(O_2/N_2)$ and CO_2 values during successive 24-h periods (thick colored line, where the line color indicates the value of the correlation coefficient). The corresponding ER values calculated from the simulated O_2 and CO_2 amount fractions by the AIST-MM with and without considering the amount fraction of cement production are shown by black solid and dotted lines, respectively. Dashed horizontal lines show the expected ER values for the consumption of

635   gas, liquid, and solid fuels (Keeling, 1988); terrestrial biospheric activities (Severinghaus, 1995); and cement production.
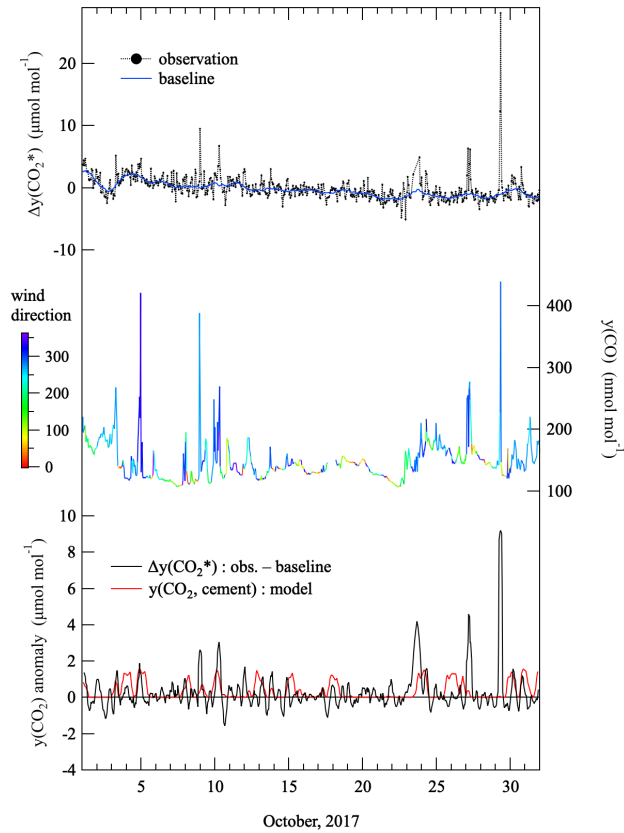
Figure 6: (top) Variations in $\Delta y(CO_2{}^*)$ calculated from the observed CO_2 amount fractions and $\delta(O_2/N_2)$ (black filled circles) in October 2017, and the baseline variation (blue solid line). Δ denotes deviations from their monthly mean values. See text for the definition of $y(CO_2{}^*)$ and the method used to obtain the baseline variation. (middle) Variations in CO amount fractions in October 2017 and the simultaneously observed wind direction (in degrees). (bottom) Five-hour-average $\Delta y(CO_2{}^*)$ anomalies from the $\Delta y(CO_2{}^*)$ baseline variation and the corresponding variation in the CO_2 amount fraction due only to cement production ($y(CO_2,$ cement)) simulated by the AIST-MM (same as the red line in the middle part of Fig. 4).
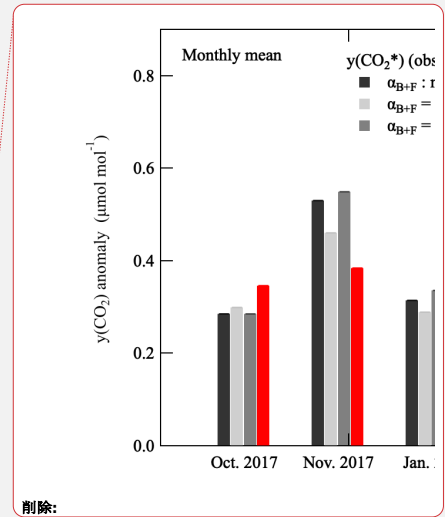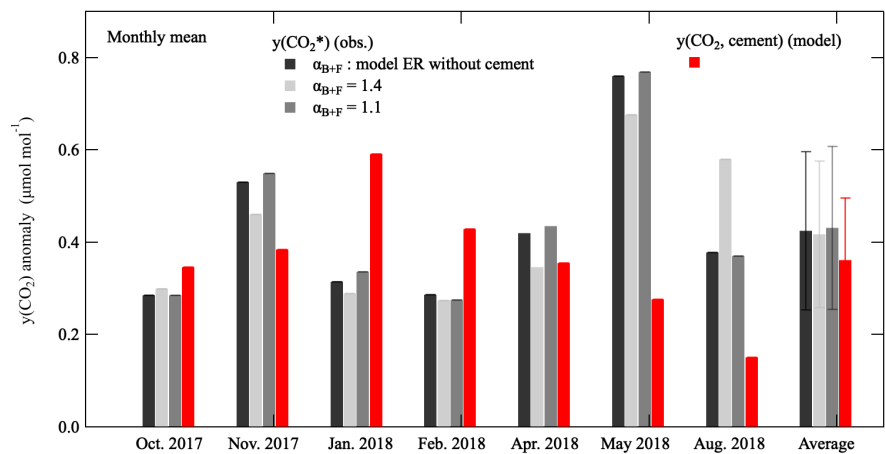
Figure 7: Monthly means of $y(CO_2^*)$ anomalies, obtained using model-simulated α_{B+F} values (as in Fig. 5a–e) and α_{B+F} values of 1.4 and 1.1, and $y(CO_2, cement)$. The monthly mean values averaged over the 5 months are shown at the right. Error bars indicate monthly variability (±1 σ).

650

削除:
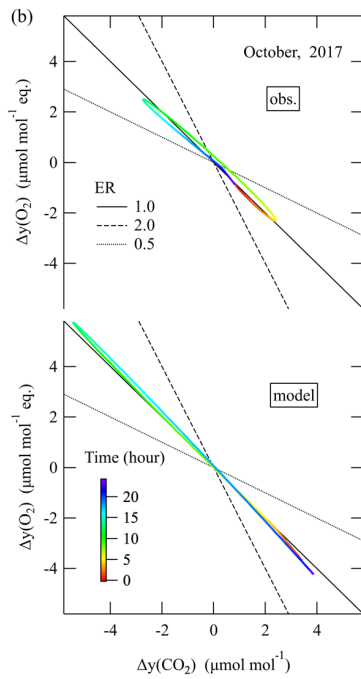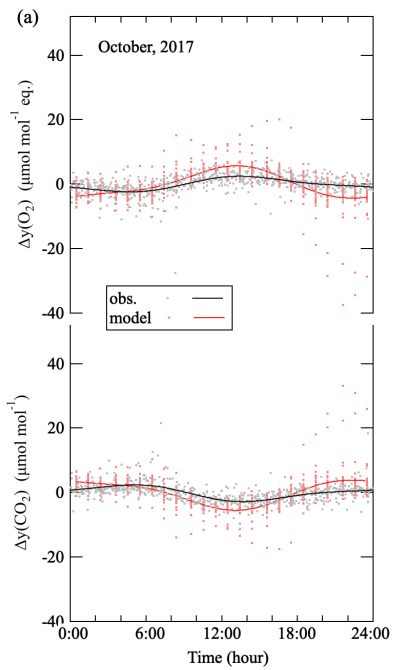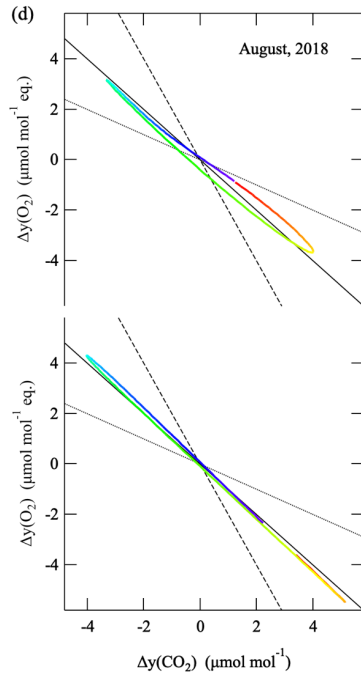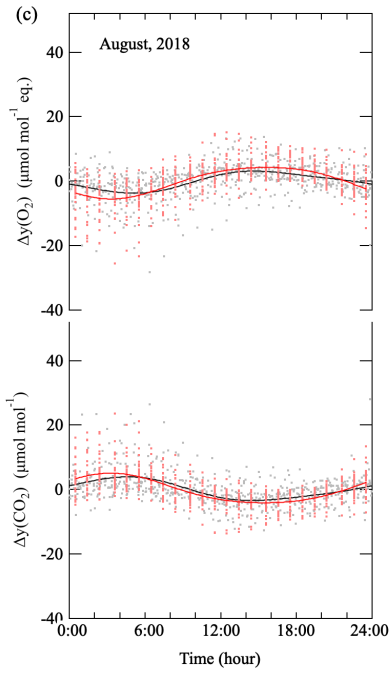
660

Figure A1: (a) Average diurnal cycles of the observed $\Delta y(O_2)$ and $\Delta y(CO_2)$ (gray dots) in October 2017. Δ denotes deviations of $\delta(O_2/N_2)$ and $y(CO_2)$ from their 24-hr mean values. The $\Delta\delta(O_2/N_2)$ was converted to $\Delta y(O_2)$ by multiplying $X(O_2)$ (=0.2094). Best-fit curves to the data, represented by the fundamental and its first harmonics (periods of 24 and 12 hours) terms, are also shown (black lines). Those of $\Delta y(O_2)$ and $\Delta y(CO_2)$ (red dots) and best-fit curves (red lines) simulated by the AIST-MM are also shown. (b)
665 Relationships between the best-fit curves of the observed (top panel) and simulated (bottom panel) $\Delta y(O_2)$ and $\Delta y(CO_2)$ shown in (a). The colour scale denotes the time of the day. The relationships expected from the ER of 1.0, 2.0 and 0.5 are also shown by black solid, dashed and dotted lines, respectively. (c) Same as in (a) but for in August 2018. (d) Same as in (b) but for in August 2018.

670

675   (a)

680

(c)

685

(d)
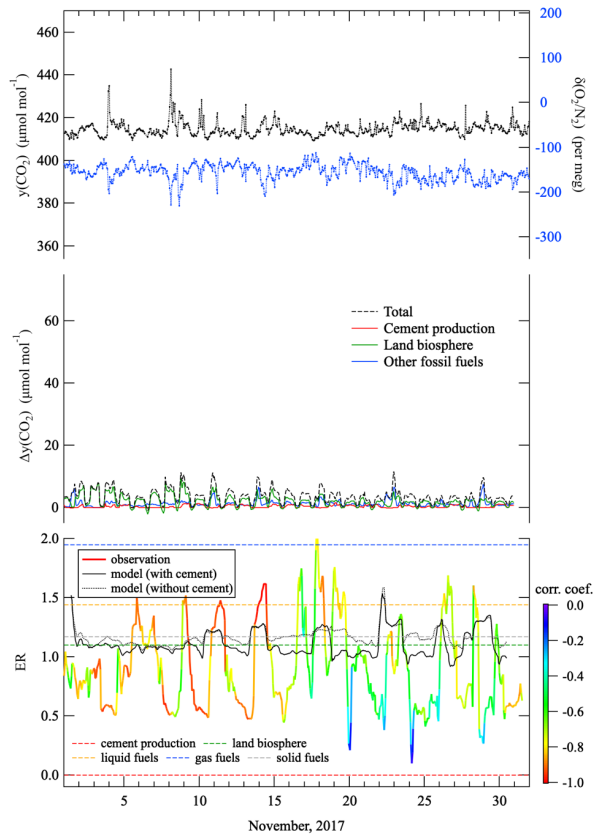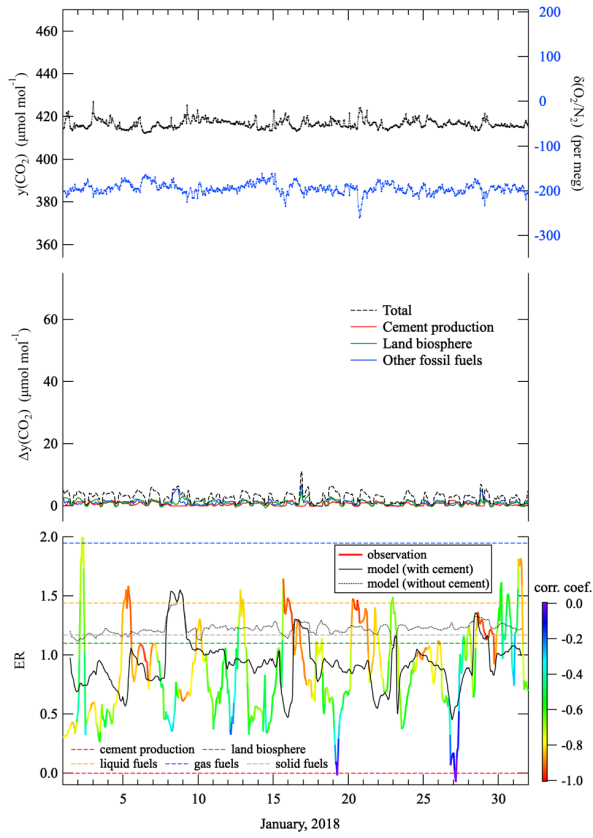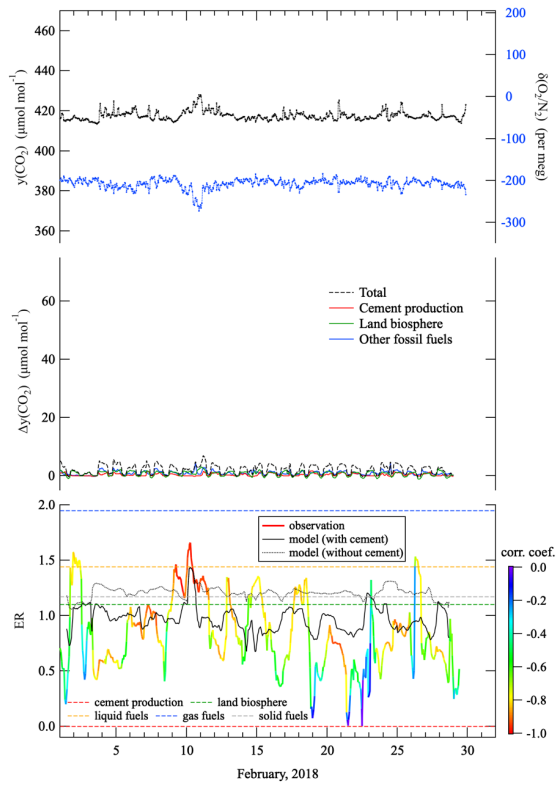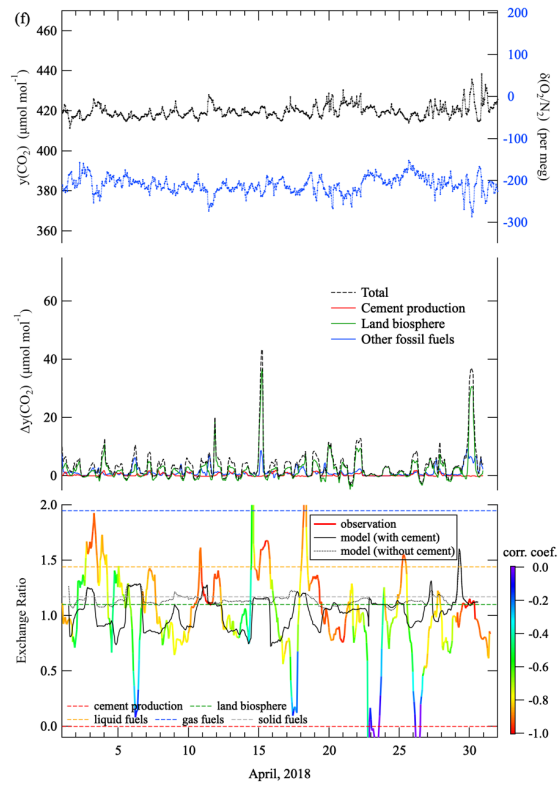
(e)
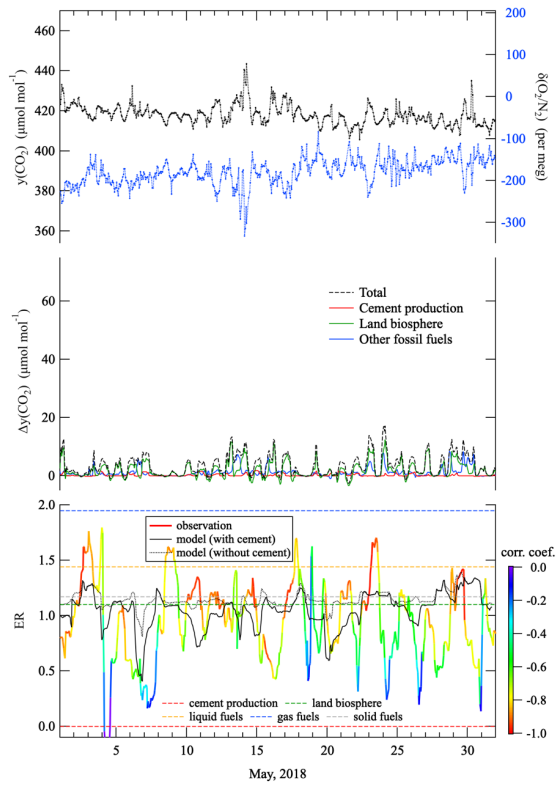
695

(f)
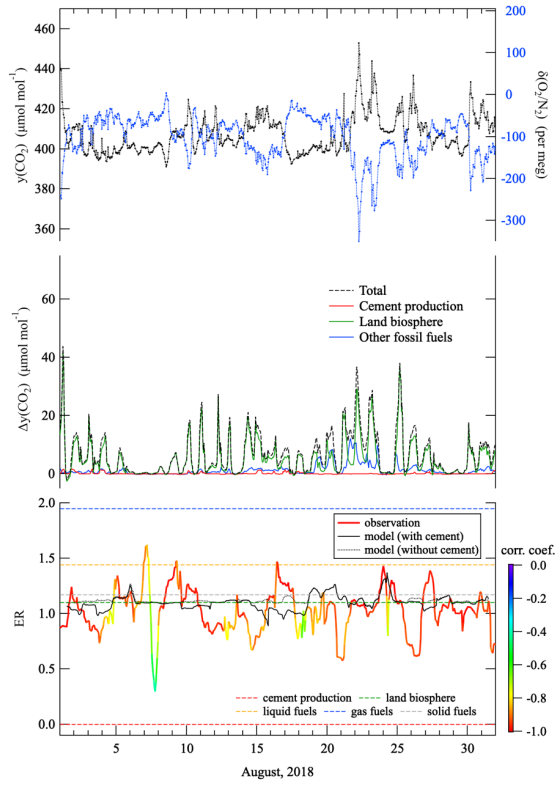
700

Figure B1: (a) Same as in Fig. 5, but for November 2017. (b) As (a), but for January, 2018. (c) As (a), but for February, 2018. (d) As (a), but for April, 2018. (e) As (a), but for May, 2018. (f) As (a), but for August, 2018.

November, 2017

(b)

February, 2018

720

(d)

(e)

730

(f)
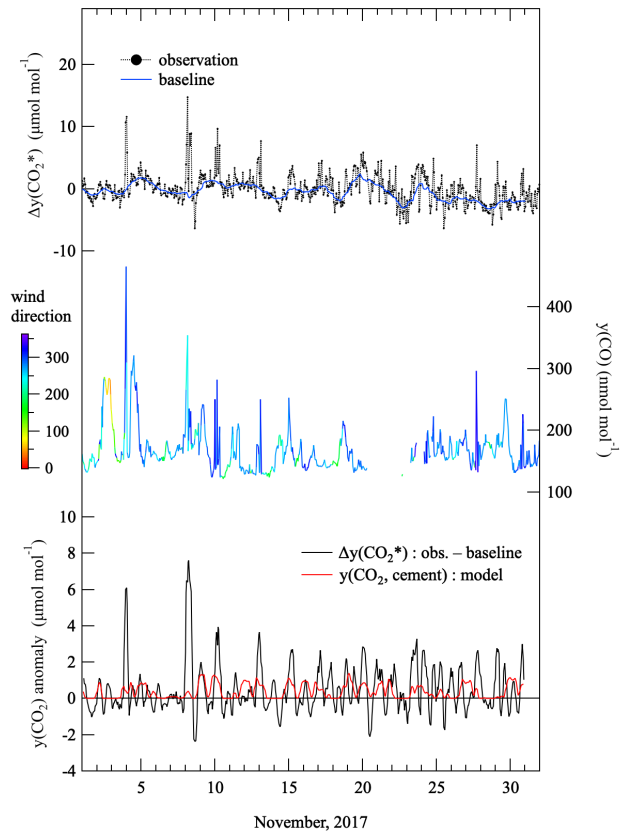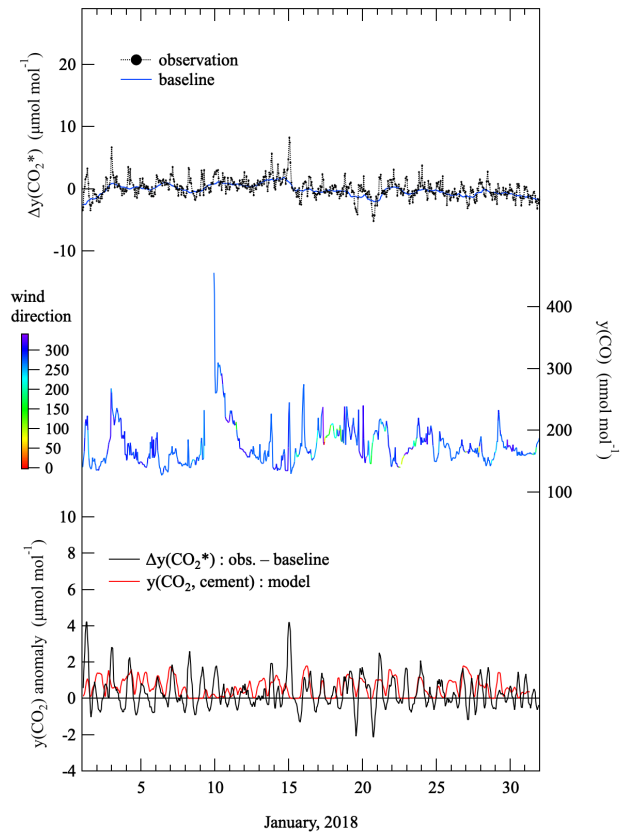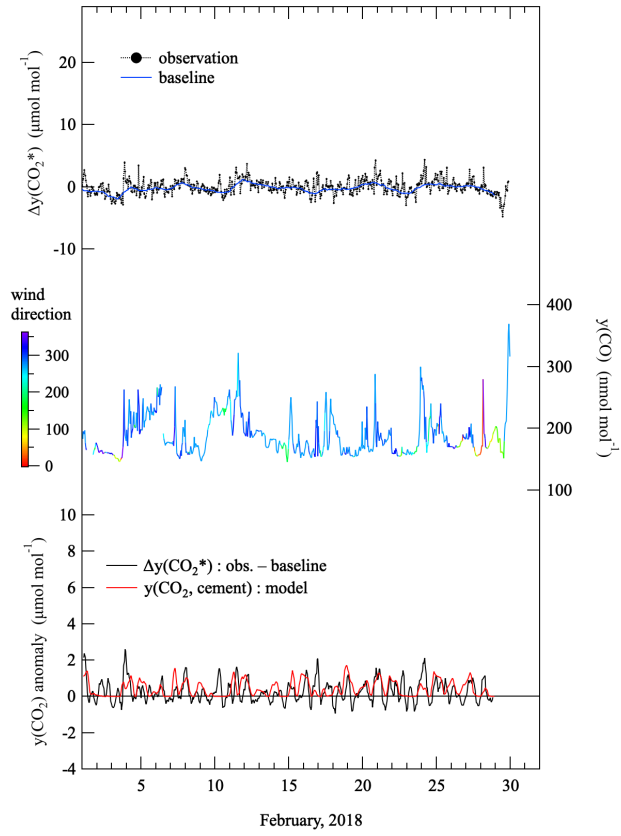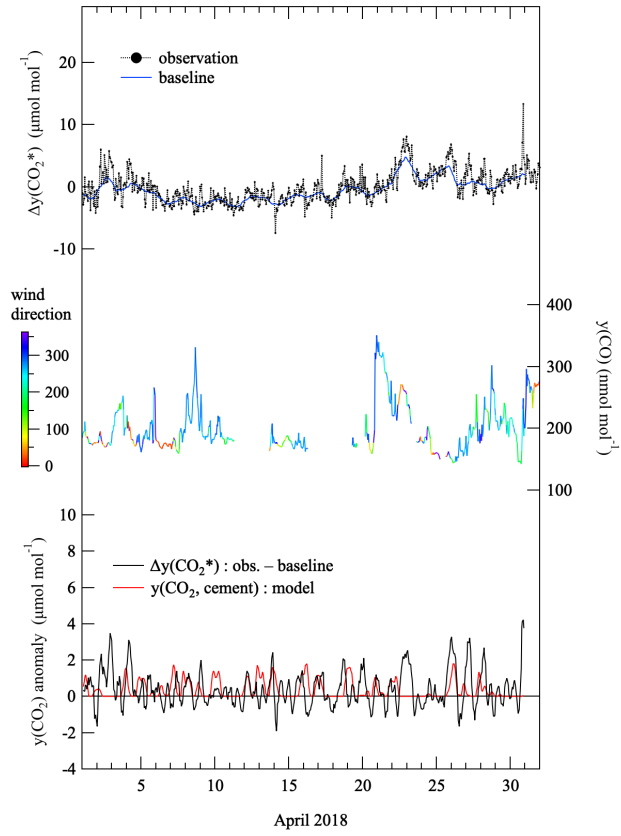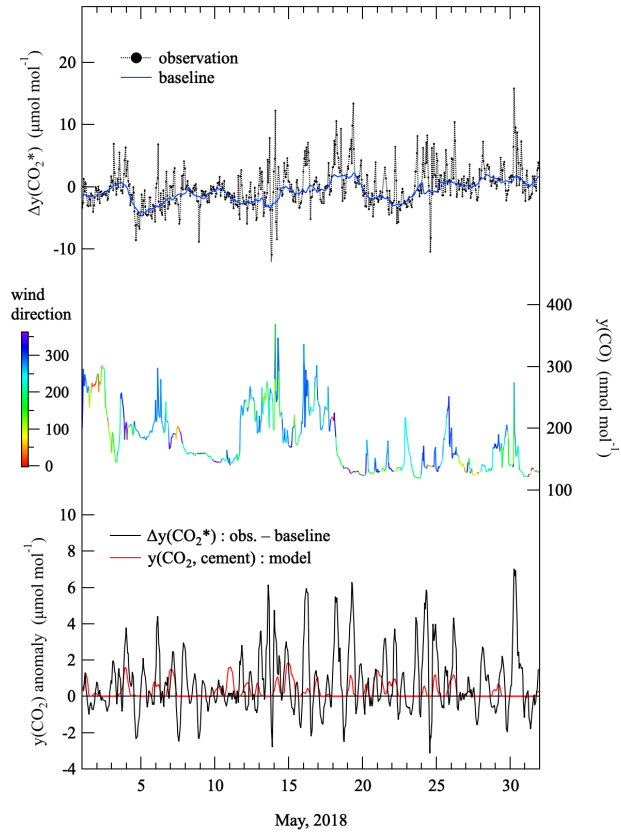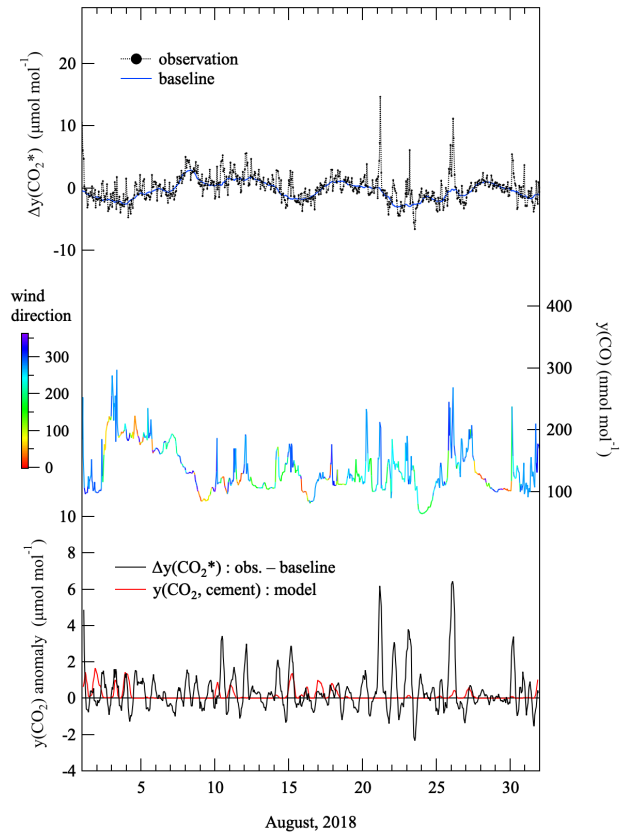
 Figure B2: (a) Same as in Fig. 6, but for November 2017. (b) As (a), but for January, 2018. (c) As (a), but for February, 2018. (d) As (a), but for April, 2018. (e) As (a), but for May, 2018. (f) As (a), but for August, 2018.

削除: A
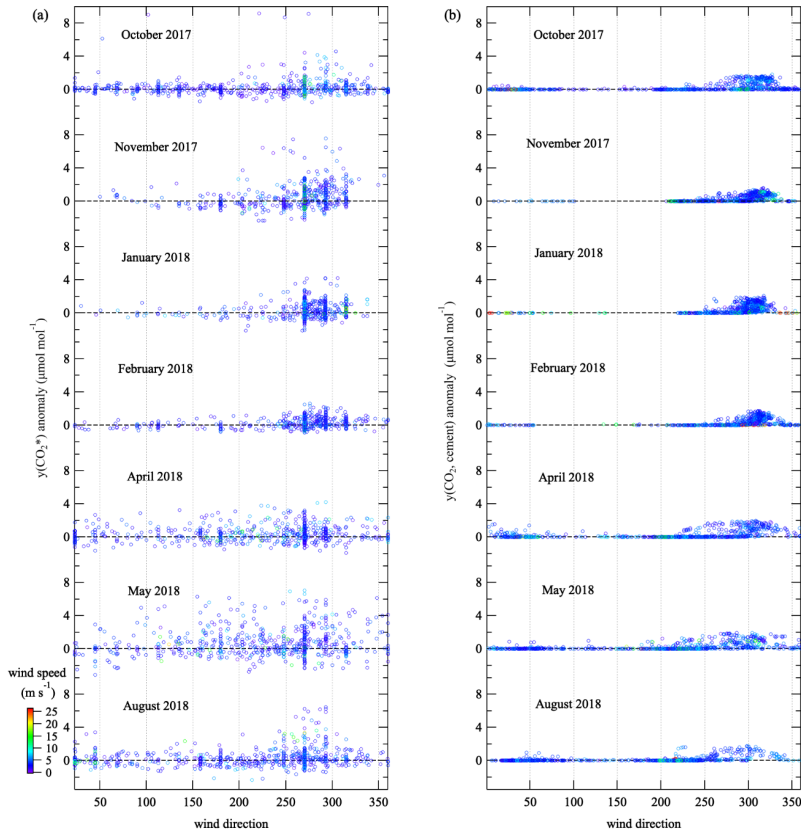
740

Figure B3: (a) Relationships between $y(CO_2^*)$ anomaly shown in Fig. 6 and Fig. B2 and wind direction at RYO. (b) Same as in (a) but for $y(CO_2, cement)$. It is noted that the $y(CO_2^*)$ anomaly are five-hour-average similar to Fig. 6 and Fig. B2 but the $y(CO_2, cement)$ are hourly values.

745

October, 2017

November, 2017
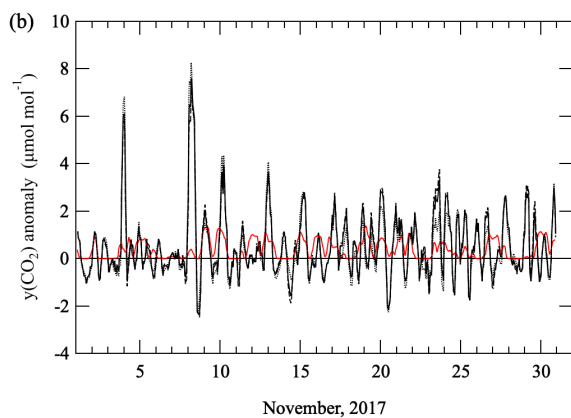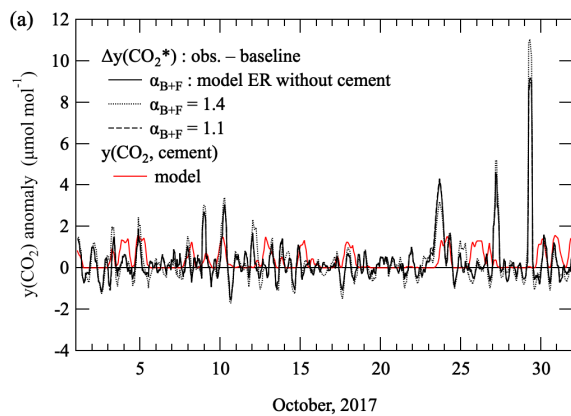
Figure B4: (a) Same as in the bottom panels of Fig. 6, but for $\Delta y(CO_2^*)$ calculated by using model-simulated α_{B+F} values (black solid line), and α_{B+F} values of 1.4 (black dotted line) and 1.1 (black dashed line). (b) Same as in (a) but for the bottom panels of Fig. B2a.